

Article

Symmetric Collaborative Fault-Tolerant Control of Multi-Intelligence under Long-Range Transmission in Air–Ground Integrated Wireless High-Mobility Self-Organizing Networks

Zhifang Wang ¹ , Mingzhe Shao ², Wenke Xu ³, Xuewei Huang ³, Yang Bai ^{3,*}, Quanzhen Huang ^{4,*} and Jianguo Yu ⁵

¹ Intelligent Investigation Research Center, Henan Police College, Zhengzhou 450046, China; wangzf124@hnp.edu.cn

² Key Cultivation Laboratory of Intelligent Transportation Policing, Henan Police College, Zhengzhou 450046, China; shaomz@hnp.edu.cn

³ Criminal Science and Technology Research Center, Henan Police College, Zhengzhou 450046, China; wenkexu@hnp.edu.cn (W.X.); huangxw@hnp.edu.cn (X.H.)

⁴ College of Electrical and Information Engineering, Henan University of Engineering, Zhengzhou 451191, China

⁵ School of Electronic Engineering, Beijing University of Posts and Telecommunications, Beijing 100876, China; yujg@bupt.edu.cn

* Correspondence: baiyang@hnp.edu.cn (Y.B.); huangquanzhen666@126.com (Q.H.)

Abstract: With the continuous development and progress of wireless self-organizing network communication technology, how to carry out long-distance cooperative control of multiple intelligences under the framework of an air–ground integrated wireless high-mobility self-organizing network has become a hot and difficult topic that needs to be solved urgently. This paper takes the air–ground integrated wireless high-mobility self-organizing network system as the basic framework and focuses on solving the long-distance cooperative fault-tolerant control of multi-intelligent bodies and the topological stability of a wireless mobile self-organizing network. To solve the above problems, a direct neural network with a robust adaptive fault-tolerant controller is designed in this paper. By constructing a symmetric population neural network model and combining it with the Lyapunov stabilization criterion, the system feedback matrix K has the ability of autonomous adaptive learning, and symmetrically distorts, rotates, or scales the training data to instantly adjust the system's fault-tolerant corrections and adaptive adjusting factors to resist the unknown disturbances and faults, to achieve the goals of multi-intelligent body stable control and the stable operation of a wireless high-mobility self-organizing network topology. Simulation results show that with the feedback adjustment of the multi-system under the designed controller, the multi-system as a whole has good fault-tolerant performance and autonomous learning approximation performance, and the tracking error asymptotically converges to zero. The experimental results show that the multi-flight subsystems fly stably, the air–ground integrated wireless high-mobility self-organizing network topology has good stability performance, and the maximum relative improvement of the topology stability performance is 50%.

Keywords: air–ground integrated wireless high-mobility self-organizing network; long-distance transmission; multi-intelligence; cooperative fault-tolerant control



Citation: Wang, Z.; Shao, M.; Xu, W.; Huang, X.; Bai, Y.; Huang, Q.; Yu, J. Symmetric Collaborative Fault-Tolerant Control of Multi-Intelligence under Long-Range Transmission in Air–Ground Integrated Wireless High-Mobility Self-Organizing Networks. *Symmetry* **2024**, *16*, 582. <https://doi.org/10.3390/sym16050582>

Academic Editor: Haitao Xu

Received: 15 March 2024

Revised: 28 April 2024

Accepted: 2 May 2024

Published: 8 May 2024



Copyright: © 2024 by the authors. Licensee MDPI, Basel, Switzerland. This article is an open access article distributed under the terms and conditions of the Creative Commons Attribution (CC BY) license (<https://creativecommons.org/licenses/by/4.0/>).

1. Introduction

With the continuous development of wireless communication technology, an air–ground integrated wireless high-mobility self-organizing network has become one of the focuses of current research [1–5]. This kind of network can achieve a high speed and high

reliability under long-distance transmission, while at the same time having the characteristics of self-organization and adaptability. However, the need for the cooperative control of multiple intelligences in the network [6,7], accompanied by various fault tolerance problems in transmission, poses a challenge for the design and optimization of the network. The cooperative control of multiple intelligences refers to cooperation and information exchange among various intelligences to achieve a common goal in an air-ground integrated wireless high-mobility self-organizing network. This coordinated control must consider each intelligent body's position, speed, transmission state, and other factors in the network to achieve efficient data transmission and rational resource utilization. However, the complexity of the wireless communication environment leads to problems such as signal attenuation, the multipath effect, and channel interference that often occur during transmission, thus reducing the reliability and transmission quality of the network. To solve these fault-tolerance problems, suitable fault-tolerance mechanisms need to be designed, including error-correction codes [7–9], retransmission mechanisms [10,11], and distributed algorithms [11,12], etc., to ensure the integrity of the data and the reliability of the transmission. This paper will explore the key technologies and methods of multi-intelligence collaborative fault-tolerant control under long-distance transmission in air-ground integrated wireless high-mobility self-organizing networks. By reasonably designing the cooperative control algorithm and fault-tolerant mechanism, the reliability and performance of the network can be improved, and technical support is provided for realizing the collaborative application of multi-intelligentsia under high-speed, long-distance transmission.

In air-ground integrated wireless high-mobility self-organizing networks, the research on the collaborative fault-tolerant control of multiple intelligences needs to address the following key issues. Collaborative control algorithms based on positional information [13–15]: The positional information of multiple intelligences is crucial for coordinated control, so it is necessary to design suitable positioning algorithms to obtain accurate positional data. Meanwhile, cooperative control algorithms based on location information can help multi-intelligentsia work together, assign tasks, and optimize resources. Fault-tolerance mechanism design [16–18]: In wireless high-mobility environments, fault tolerance problems such as channel interference and multipath effects are common. To improve the reliability and robustness of the network, adaptive fault-tolerance mechanisms need to be designed, including error detection [18,19], correction codes [20,21], and adaptive retransmission [22,23]. These fault-tolerant mechanisms can help multi-intelligentsia to recover and retransmit data in the face of errors and interferences in transmission, ensuring data integrity and reliability. Distributed decision-making and cooperative control strategies [24–26]: In the cooperative control of multiple intelligences, decision-making and cooperative management need to be carried out by taking into account information such as the position and transmission state of each intelligence. Distributed algorithms and collaborative control strategies can enable multi-intelligentsia to adaptively perform task allocation, resource optimization, and decision-making, thus improving the performance and efficiency of the whole network. By solving the above fundamental problems and considering the characteristics of wireless high-mobility self-organizing networks, the effect of the cooperative fault-tolerant control of multiple intelligences can be improved to achieve high speed and high reliability under long-distance transmission. This will provide more stable and reliable communication support for future multi-intelligent body applications and promote the development of wireless communication technology and the wide application of applications.

In summary, this paper takes the air-ground integrated wireless high-mobility self-organizing network system as the primary research object. It takes the internal actuator faults of multi-flying intelligences (including two types of defects: sudden interruption and partial failure of actuators) and wireless communication faults of wireless self-organizing network association links between multi intelligences (including two types of faults: data transmission delay and packet loss of wireless self-organizing network) as well as external unknown interference as the system perturbation fault information in the process of long-

distance network transmission. With strange interference as the system perturbation fault information, the distributed robust adaptive neural network cooperative fault-tolerant controller is proposed for the multi-intelligent bodies of this system, so that the system as a whole has good group robust performance, cluster adaptive regulation performance, autonomous learning performance, and fault-tolerance performance.

Special Note 1: The research objective of this paper is the air-ground integrated wireless mobile self-organizing network; the network nodes in this network system have direct symmetry or peer-to-peer. (1) All nodes in the network can act as receivers and senders in group communication, and this symmetrical structure can enable all nodes to have the same communication capability. (2) The nodes in the network collaborate to find the best communication path. (3) All nodes can share each other's resources, such as bandwidth, storage space, etc. The symmetric network architecture can promote deep cooperation between nodes and the full utilization of resources. (4) The symmetric network structure makes each network node self-consistent, independent, and self-contained, and it can intelligently decide whether to join or leave the network according to its needs, without the need for central node control and management. The cooperative symmetric fault-tolerant controller designed in this paper for multiple intelligences has symmetry: (1) The neural network in the controller has a symmetric structure, and the symmetric inter-layer connections can reduce the single point of failure in the network so that even if part of the connections or nodes are damaged, the network as a whole can still operate normally. (2) The neural networks in the controller have the same convolutional kernel to share parameters, improving the generalization ability of the controller model. (3) Symmetrically twisting, rotating, or scaling the training data can make the model more robust to different transformations. (4) Reducing the amount of fitted data simulation computation by randomly and symmetrically dropping a portion of the nodes or connections during the training and learning process makes the system network fault-tolerant to the loss of all or loss of some nodes. The relationship between the "air-ground self-organizing network system" and the "air-ground self-organizing network subsystem" is inclusive. From a macroscopic point of view, the network system studied in this paper is homogeneous, and the difference is reflected in the internal uncertainty.

2. Modeling of the Whole System

Consider an integrated system A_G consisting of N consecutive air-ground wireless self-organizing network subsystems A_{Gi} , $i = 1, 2, \dots, N$. (v_{wj}, v_{wi}) is used to denote a corresponding usually valid air-ground wireless self-organizing network association link from the air-ground wireless self-organizing network system i to j where each air-ground wireless self-organizing network subsystem is represented by the state equation shown in Equation (1).

$$\begin{aligned} \frac{dx_i(t)}{dt} = & Ax_i(t) + \sum_{j=1, i \neq j}^N a_{ij} A_1 [x_j(t) - x_i(t) + d_{ij}(t)] \\ & + B_2 [\beta u_i(t) + f_{ni}(t)] + B_1 \omega_i(t) + \Delta(t) \end{aligned} \quad (1)$$

In Equation (1), $x_i(t) \in R^n$ denotes the state of the i th open space wireless self-organizing network subsystem. $u_i(t) \in R^q$ indicates the control input of the system as a whole. $a_{ij} \in R$ denotes the networking topology of the air-ground wireless self-organizing network, represented as an element of the Laplace matrix, $a_{ii} + \sum_{i \neq j, j=1}^N a_{ij} = 0$. $A_1 \in R^{n \times n}$ denotes the actuator coupling matrix within the system, describing the associative links between actuators. $d_{ij} \in R^n$ denotes the wireless self-organizing network association link failure perturbation between the i th air-ground wireless self-organizing network subsystem and the j th air-ground wireless self-organizing network subsystem that satisfies $\underline{d}_{ij} \leq d_{ij} \leq \bar{d}_{ij}$, where \underline{d}_{ij} and \bar{d}_{ij} represent the lower and upper bound amplitudes of d_{ij} , respectively. $f_{ni}(t)$ denotes the nonlinear equation in the air-ground wireless self-organizing network system defined between the lower and upper bound amplitudes of the

unknown $f_{-ni}(t), \bar{f}_{ni}(t)$. $\omega_i(t) \in L_2^m[0, \infty)$ represents a continuous energy-bounded signal indicating unknown external perturbations and possible changes in the typical parameter values corresponding to the air-ground wireless self-organizing network system. $\Delta(t)$ denotes a superficial strange concern of the air-ground wireless self-organizing network system. β represents the unknown nonlinear function. Here, all system matrices are known constant matrices with proper dimensions. Then, Kronecker's inner product is introduced, and then Equation (1) can be expressed as Equation (2).

$$\begin{aligned} \frac{dx_i(t)}{dt} = & [I \otimes A + L \otimes A_1]x(t) + (I \otimes A_1)d(t) \\ & + (I \otimes B_2)\beta u(t) + (I \otimes B_2)f_{ni}(t) + (I \otimes B_1)\omega(t) \\ & + (I \otimes I)\Delta(t) \end{aligned} \quad (2)$$

In Equation (2), $x = (x_1^T, \dots, x_N^T)^T$, $u = (u_1^T, \dots, u_N^T)^T$, $f = (f_1^T, \dots, f_N^T)^T$, $\omega = (\omega_1^T, \dots, \omega_N^T)^T$, $d = (d_1^T, \dots, d_N^T)^T$, $\Delta = (\Delta_1^T, \dots, \Delta_N^T)^T$, $d_i(t) = \sum_{i \neq j, j=1}^N a_{ij}d_{ij}$, $i = 1, 2, \dots, N$. L denotes the Laplace matrix, defined as shown in Equation (3).

$$l_{ij} = \begin{cases} -\sum_{k \neq i, k=1}^N a_{ik}, & i \neq j \\ a_{ij}, & i = j \end{cases} \quad (3)$$

To ensure the average convergence objective, the following Assumptions 1–3 are given. The average convergence objective refers to the eventual asymptotic stabilization of the overall network system under the feedback regulation of the designed controller.

Assumption 1. For the air-ground wireless self-organizing network integrated system Equation (2) and any proper dimension matrix Q , there exist matrix equations W and Z of appropriate dimension such that Equation (4) holds.

$$\begin{cases} A = B_2Z \\ A_1 + B_2Q = B_2W \end{cases} \quad (4)$$

The following definition is then made such that $\alpha = \frac{1}{N} \sum_{i=1}^N x_i(0)$, where $x_i(0)$, $i = 1, 2, \dots, N$ denotes the initial value of the known system state.

A discussion of "Assumption 1" begins with the uncertainty that the matrices Z and W are expressions of a class of nonlinear equations. Equation (4) gives a strong assumption on the uncertainty of the control input matrix of the network system while relaxing the existing assumptions on the uptake of the system. If $A_1 = 0$, then there is a degeneration of Equation (4) to a vanilla-bounded uncertainty term. In addition, "Assumption 1" is a standard assumption for defining matching conditions for model matching control, which can address the average convergence of the network system under internal actuator failures and link perturbations.

Assumption 2. β is known and $\beta(x) \neq 0$. A general conclusion exists for any $x \in R$, and we assume $\beta > 0$.

Assumption 3. There exists a smooth trace function β_t such that $|\beta(x)| \leq \beta_t$. And, a smooth trace function is a function for which all finite order derivatives exist in the domain of definition.

Special Note 2: Compared to the traditional adaptive fault-tolerant controllers designed for associated link and actuator failure faults in distributed systems, they involve a limited number of faults, many estimation parameters, and a heavy computer computational burden. In this paper, we consider the more general associated link and internal actuator failures, where "Assumption 1" and "Assumption 2" are the standard assumptions for defining the matching conditions for the mathematical model matching control, and "Assumption 3" are also standard assumptions. The standard assumptions are generally

not restricted by limiting conditions. In addition, since the controller designed in this paper targets multiple intelligences, it contains two separate parts, one for robust adaptive fault-tolerant parameter settings and one for neural-network-related parameter settings. Among them, Assumption 1 addresses the robust adaptive fault-tolerant control part, and Assumptions 2 and 3 address the neural network adaptive regulation part. While overall without loss of generality Assumptions 2 and 3 appear to be negligible, the assumptions corresponding to the use of the relevant parameters in the neural network adaptive regulation part should not be completely ignored.

To solve the problem of the stable convergence of the air-ground wireless self-organized network system under the unknown control faults of the internal actuators, the unknown communication faults of the air wireless self-organized network associated with the ground wireless self-organized network link failure, and the unknown external perturbations, this paper proposes a direct neural network robust and adaptive fault-tolerant control law shown in Equation (5).

$$\begin{cases} u_i(t) = -Q \left[\sum_{i \neq j, j=1}^N a_{ij} [x_i(t) - x_j(t) + d_{ij}] + c_i [x_i(t) - \alpha] \right] \\ + v_i(t) - \Gamma_N [z(t) E_{err} + \sigma \hat{W}_F] \\ i, j = 1, \dots, N \end{cases} \quad (5)$$

In Equation (5), a_{ij} is defined in Equation (1). c_i denotes a positive constant. Q indicates the control gain equation. $v_i(t)$ displays the multi-task cooperative robust adaptive fault-tolerant control equation to be designed subsequently in this paper. $\Gamma_N = \Gamma_N^T > 0$ indicates the multi-task neural network adaptive gain matrix. $\sigma > 0$ indicates the constant number. \hat{W}_F indicates the estimation of the weight value \hat{W}_F^* of the ideal multi-task air-ground wireless self-organizing network. $z(t)$ represents the Gaussian radial function vector. Here, the perfect tracking control signal vector of the air-ground wireless self-organizing network system is defined as x_{ideal} . The tracking error of the system is e_{rr} . The tracking error function of the system is E_{err} . Then, it satisfies Equation (6) and holds.

$$\begin{cases} x_{ideal} = \left[x_{ideal1}, \frac{dx_{ideal1}}{dt}, \dots, x_{idealN}, \frac{dx_{idealN}}{dt} \right]^T \\ e_{rr} = \Delta x = x - x_{ideal} = \left[e_{rr1}, \frac{de_{rr1}}{dt}, \dots, e_{rrN}, \frac{de_{rrN}}{dt} \right] \\ E_{err} = [\lambda, 1] e_{rr} = \lambda e_{rr} + \frac{de_{rr}}{dt} \end{cases} \quad (6)$$

In Equation (6), λ denotes a constant greater than zero. Then, using Kronecker's inner product, Equation (5) can be written as Equation (7).

$$\begin{aligned} u(t) = & -(L + C_N) \otimes Qx(t) + C_N \otimes (Q\alpha) + (I \otimes Q)d + v \\ & - C_N \otimes \Gamma_N [z(t)(I \otimes E_{err}) + \sigma(I \otimes \hat{W}_F)] \end{aligned} \quad (7)$$

Substituting Equation (7) into Equation (2), we have the closed-loop system model which becomes Equation (8).

$$\begin{aligned} \frac{dx(t)}{dt} = & [I \otimes A + L \otimes A_1]x(t) + (I \otimes B_2)f(t) \\ & + (I \otimes B_1)\omega(t) + (I \otimes I)\Delta(t) - (L + C_N) \otimes (B_2Q\alpha)\beta \\ & + [I(A_1 + \beta B_2Q)]d(t) + (I \otimes B_2)\beta v(t) \\ & - C_N \otimes (B_2\Gamma_N) [z(t)(I \otimes E_{err}) + \sigma(I \otimes \hat{W}_F)]\beta \end{aligned} \quad (8)$$

Next, let $\Delta x(t) = x(t) - \alpha$. With the characterization of the Laplacian matrix, Equation (9) holds.

$$(L + C_N) \otimes Q[x(t) - \alpha] = (L + C_N) \otimes Qx - C_N \otimes (Q\alpha) \quad (9)$$

According to Equation (9), Equation (10) can be obtained by substituting $\Delta x(t)$ into Equation (8).

$$\begin{aligned} \frac{d\Delta x(t)}{dt} &= (I \otimes B_2)f(t) + (I \otimes B_1)\omega(t) + (I \otimes I)\Delta(t) \\ &+ [I(A_1 + \beta B_2 Q)]d(t) + C_N \otimes (B_2 Q \alpha)\beta + (I \otimes B_2)\beta u(t) \\ &- C_N \otimes (B_2 \Gamma_N) [z(t)(I \otimes E_{err}) + \sigma(I \otimes \hat{W}_F)]\beta \\ &- [I \otimes A + L \otimes A_1 - \beta(I \otimes B_2)(L + C_N) \otimes Q]\Delta x(t) \end{aligned} \quad (10)$$

According to Assumption 1, Equation (10) can be rewritten as Equation (11).

$$\begin{aligned} \frac{d\Delta x(t)}{dt} &= (I \otimes B_2)\beta v(t) + (I \otimes B_1)\omega(t) + (I \otimes I)\Delta(t) \\ &- C_N \otimes (B_2 \Gamma_N) [z(t)(I \otimes E_{err}) + \sigma(I \otimes \hat{W}_F)]\beta \\ &- [I \otimes A + L \otimes A_1 - \beta(I \otimes B_2)(L + C_N) \otimes Q]\Delta x(t) \\ &+ (I \otimes B_2)e_s(t) \end{aligned} \quad (11)$$

In Equation (11), $C_N = \text{diag}(c_i)$, $e_s = [e_1^T, \dots, e_N^T]^T$, $e_{si}(t) = f_{ni}(t) + Wd_i(t) + Z\alpha$. Here, since $f_{ni}(t)$, $d_i(t)$, and α are bounded wireless self-organizing network signals, define \underline{e}_{si} and \bar{e}_{si} as unknown constants larger than the lower and upper bounds of e_{si} , respectively.

To ensure that the system Equation (11) is asymptotically stabilized in the presence of air-ground wireless self-organizing network perturbations associated with link failures, unknown internal actuator failures, and unknown external concerns, there exists Equation (12) that holds.

$$\begin{cases} \lim_{t \rightarrow \infty} \Delta x(t) = 0 \\ \lim_{t \rightarrow \infty} x(t) = \alpha \end{cases} \quad (12)$$

In Equation (12), $\lim_{t \rightarrow \infty} \Delta x(t) = 0$ denotes that the network system (11) is asymptotically stabilized under an associated perturbation link and an unknown failure of an internal actuator. $\lim_{t \rightarrow \infty} x(t) = \alpha$ denotes that the network system (11) has the L_2 performance metric.

3. Robust Adaptive Fault-Tolerant Controller Design for Multiple Intelligences

For the above closed-loop system, the composite robust adaptive sliding mode surface shown in Equation (13) is given in this paper.

$$s_{slide}[\Delta x(t)] = 0 \quad (13)$$

In Equation (13), the relevant definition is shown in Equation (14).

$$s_{slide}[\Delta x(t)] \equiv: [s_{slide1}(\Delta x_1(t)), \dots, s_{slideN}(\Delta x_N(t))]^T \quad (14)$$

And, the relevant definitions in Equations (13) and (14) are shown in Equation (15).

$$s_{slidei}[\Delta x_i(t)] = \Delta x_i(t) - \Delta x_i(t_0) - \int_0^t \left\{ \begin{array}{l} \left[A\Delta x_i(\tau) + \sum_{i \neq j, j=1}^N a_{ij}A_1[\Delta x_j(\tau) - \Delta x_i(\tau)] \right] \\ -B_2Q_1 \left[\sum_{i \neq j, j=1}^N a_{ij}[\Delta x_j(\tau) - \Delta x_i(\tau)] + c_i\Delta x_i(\tau) \right] \end{array} \right\} d\tau \quad (15)$$

In Equation (15), Q_1 is the control gain matrix in Equation (5) and can be obtained by solving the LMI matrix Equation (16).

$$\begin{aligned} &[I \otimes A + L \otimes A_1 - \beta(I \otimes B_2)(L + C_N) \otimes Q_1]^T (I \otimes P) \\ &+ (I \otimes P)[I \otimes A + L \otimes A_1 - \beta(I \otimes B_2)(L + C_N) \otimes Q_1] < 0 \end{aligned} \quad (16)$$

In Equation (16), P denotes the positive definite matrix and the control gain matrix Q_1 is designed to stabilize the regular air-ground wireless self-organizing network fault-free integrated system. Next, consider the control gain Q_1 resolved in Equation (16) by the air-ground wireless self-organizing network combined system Equation (5), and design the controller as shown in Equation (17).

$$u_i = \hat{\Omega}_i \|s_{l_{idei}} P B_2\| \operatorname{sgn}(s_{l_{idei}}^T P B_2)^T + Q_2 [(I - \rho_i) \hat{e}_{si}(t) + \rho_i \underline{e}_{si}(t)] - \left[\frac{1}{\varepsilon \beta(x)} + \frac{1}{\varepsilon \beta^2(x)} - \frac{1}{2\beta^2(x)} \cdot \frac{d\beta(x)}{dt} \right] E_{err} - \frac{1}{\beta(x)} [\alpha(t) + \gamma] \quad (17)$$

In Equation (17), Ω_i is an existent unknown sufficiently large positive constant satisfying Equation (18).

$$2\Omega_i \|s_{l_{idei}} P B_2\|^2 \geq \|s_{l_{idei}} P B_1\|^2 + \gamma_i \|s_{l_{idei}}\|^2 \quad (18)$$

In Equation (18), γ_i is any given performance parameter. $\hat{\Omega}_i$ denotes the estimation of Ω_i , which is regulated by the robust adaptive law of the neural network shown in Equation (19).

$$\frac{d\hat{\Omega}_i(t)}{dt} = \gamma_i \|s_{l_{idei}} P B_2\|^2 \quad (19)$$

In Equation (19), $\gamma_i > 0$ denotes the weighting coefficient of the robust adaptive fault-tolerant regulation law $\hat{\Omega}_i$ of the direct neural network. The symbolic equation $\operatorname{sgn}(s_{l_{idei}}^T P B_2)^T = [\operatorname{sgn}(b_{i1}), \dots, \operatorname{sgn}(b_{iq})]^T$, where $b_{il}, l = 1, 2, \dots, q$ is the l th element of the vector $s_{l_{idei}}^T P B_2$ and $\operatorname{sgn}(b_{il})$ is defined as shown in Equation (20).

$$\operatorname{sgn}(b_{il}) = \begin{cases} -1, & b_{il} > 0 \\ 1, & b_{il} < 0 \\ 0, & b_{il} = 0 \end{cases} \quad (20)$$

Next, the direct neural network moderator is introduced into Equation (17), which leads to Equation (21).

$$u_i = \hat{\Omega}_i \|s_{l_{idei}} P B_2\| \operatorname{sgn}(s_{l_{idei}}^T P B_2)^T + Q_2 [(I - \rho_i) \hat{e}_{si}(t) + \rho_i \underline{e}_{si}(t)] + \beta(x) (\Delta \hat{W}^T z(t) - \mu_{NI}) - \left[\frac{1}{\varepsilon \beta(x)} + \frac{1}{\varepsilon \beta^2(x)} - \frac{1}{2\beta^2(x)} \cdot \frac{d\beta(x)}{dt} \right] E_{err} \quad (21)$$

In Equation (21), $\beta(x)$ is the coefficient of $\Delta \hat{W}^T$, $\Delta \hat{W}^T = \hat{W} - W^*$. $z(t)$ is the Gaussian radial basis function vector. μ_{NI} denotes the approximation error of the direct neural network, which satisfies $|\mu_{NI}| \leq \mu_{N0}$. \hat{W} indicates the estimation of the ideal weights W^* for the air-ground wireless self-organizing network. P is a positive definite symmetric matrix designed in Equation (16). ρ_i characterizes as the robust adaptive fault tolerant switching factor of the neural network between constant values 0 and 1, as shown in Equation (22).

$$\begin{cases} \rho_i = \operatorname{diag}[\rho_{i1}, \dots, \rho_{iq}] \\ \rho_{il} = \begin{cases} 0, & b_{il} \geq 0 \\ 1, & b_{il} < 0 \end{cases} \end{cases} \quad (22)$$

$\hat{e}_{sil}(t)$ and $\underline{e}_{sil}(t)$ are the estimates of $\bar{e}_{il}(t)$ and $\underline{e}_{il}(t)$, respectively, which are upgraded by the direct neural network robust adaptive fault tolerance law shown in Equation (23).

$$\begin{cases} \frac{d\hat{e}_{sil}(t)}{dt} = \zeta_{il \max} b_{il} \\ \frac{d\underline{e}_{sil}(t)}{dt} = \zeta_{il \min} b_{il} \end{cases} \quad (23)$$

In Equation (23), both $\zeta_{il\min}, \zeta_{il\max} > 0$ are the robust adaptive fault-tolerant gains of the direct neural network designed through the operation of the air-ground wireless self-organizing network system. Then, Equation (24) is given.

$$\begin{cases} \Delta\Omega_i(t) = \hat{\Omega}_i(t) - \Omega_i \\ \Delta\bar{e}_{si}(t) = \hat{\bar{e}}_{si}(t) - \bar{e}_{si} \\ \Delta\underline{e}_{si}(t) = \hat{\underline{e}}_{si}(t) - \underline{e}_{si} \end{cases} \quad (24)$$

For Equation (24), the relevant parameters are defined in Equation (25).

$$\begin{cases} \bar{e}_{si} = [\bar{e}_{si1}, \dots, \bar{e}_{siN}]^T \\ \underline{e}_{si} = [\underline{e}_{si1}, \dots, \underline{e}_{siN}]^T \\ i = 1, 2, \dots, N \end{cases} \quad (25)$$

Since both $\Omega_i, \bar{e}_{si}, \underline{e}_{si}$ are constants, the error system shown in Equation (26) can be obtained.

$$\begin{cases} \frac{d\Delta\Omega_i}{dt} = \frac{d\hat{\Omega}_i}{dt} \\ \frac{d\Delta\bar{e}_{si}}{dt} = \frac{d\hat{\bar{e}}_{si}}{dt} \\ \frac{d\Delta\underline{e}_{si}}{dt} = \frac{d\hat{\underline{e}}_{si}}{dt} \end{cases} \quad (26)$$

For the air-ground wireless self-organizing network system Equation (11), the direct neural network robust adaptive fault-tolerant control strategy equation is proposed, and the control gain Q_2 is shown in Equation (27).

$$-Q_2 = I \quad (27)$$

As a result, the following theorem is given in this paper to ensure the consistent stabilization of the closed-loop system and error system of the dynamic closed-loop periodic and error system of air-ground wireless self-organizing network is bounded.

Theorem 1. *Considering the air-ground wireless self-organizing network closed-loop system Equation (11) satisfies Assumptions 1–3, and using the control strategy expressed in Equation (7), the direct neural network robust adaptive fault-tolerance law Equation (19), and the control gain Equation (28), then it can be guaranteed that all the signals of the air-ground wireless self-organizing network sub-closed-loop system are bounded and satisfy $\lim_{t \rightarrow \infty} x_i(t) = \alpha$ for any initial value of $x(t)|_{t=0}$, and the system has an arbitrary L_2 performance gain metric γ_i , and it is assumed that there exists a positive definite matrix $P > 0$ satisfying Equation (16). The following proof procedure is then given.*

Proof. First, for the air-ground wireless self-organizing network closed-loop system Equation (11), define the following Lyapunov generalized function as shown in Equation (28).

$$V(t) = V_1(t) + V_2(t) \quad (28)$$

In Equation (28), the relevant parameters are shown in Equation (29).

$$\begin{cases} V_1(t) = s_{lide}^T (I \otimes P) s_{lide} + \sum_{i=1}^N \frac{\Delta\Omega_i^2}{\gamma_i} \\ + \sum_{i=1}^N \sum_{j=1}^n \frac{(1-\rho_{ij})\Delta\bar{e}_{sil}^2}{\zeta_{il\max}} + \sum_{i=1}^N \sum_{j=1}^n \frac{\rho_{ij}\Delta\underline{e}_{sil}^2}{\zeta_{il\min}} \\ V_2(t) = \frac{1}{2} \left[\frac{E_{err}}{\beta(x)} + \Delta W_F^T \Gamma^{-1} \Delta W_F \right] \end{cases} \quad (29)$$

According to Assumptions 1–3, the derivative of $V(t)$ with respect to time t when $t > 0$ is shown in Equation (30).

$$\frac{dV(t)}{dt} = \frac{dV_1(t)}{dt} + \frac{dV_2(t)}{dt} \quad (30)$$

In Equation (30), the relevant parameters are defined as shown in Equations (31) and (32).

$$\begin{aligned} \frac{dV_1(t)}{dt} &= 2 \sum_{i=1}^N \hat{\Omega}_i \|s_{lide}^T PB_2\| s_{lide}^T + 2 \sum_{i=1}^N s_{lide} PB_1 \omega_i \\ &+ 2s_{lide}^T (I \otimes P) \sum_{i=1}^N \sum_{l=1}^n B_i e_{sil} \\ &+ 2s_{lide}^T (I \otimes P) \sum_{i=1}^N \sum_{l=1}^n B_i k_{2l} (\hat{e}_{sil} + \rho_{il} \hat{e}_{sil} - \rho_{il} \hat{e}_{sil}) \\ &+ \sum_{i=1}^N \frac{2\Delta\Omega_i}{\gamma_i} \cdot \frac{d\Delta\Omega_i}{dt} + \sum_{i=1}^N \sum_{l=1}^n \frac{2(1-\rho_{il})\Delta\bar{e}_{sil}}{\xi_{ilmax}} \cdot \frac{d\Delta\bar{e}_{sil}}{dt} \\ &+ \sum_{i=1}^N \sum_{l=1}^n \frac{2\rho_{il}\Delta e_{sil}}{\xi_{ilmin}} \cdot \frac{d\Delta e_{sil}}{dt} \end{aligned} \quad (31)$$

In Equation (31), B_i is the i th column of $I \otimes B_2$.

$$\begin{aligned} \frac{dV_2(t)}{dt} &= - \left[\frac{1}{\varepsilon\beta(x)} + \frac{1}{\varepsilon\beta^2(x)} \right] E_{err}^2 + \frac{d(t)}{\beta(x)} E_{err} \\ &- \mu_{Nl} E_{err} - \sigma \Delta W_F^T \dot{W}_F \end{aligned} \quad (32)$$

Against $\frac{dV_1(t)}{dt}$, it can be noted that Equation (33) holds.

$$\begin{aligned} &s_{lide}^T (I \otimes P) \sum_{i=1}^N \sum_{l=1}^n B_i e_{sil} \\ &\leq s_{lide}^T (I \otimes P) \sum_{i=1}^N \sum_{l=1}^n B_i (\bar{e}_{sil} + \rho_{il} e_{sil} - \rho_{il} \bar{e}_{sil}) \end{aligned} \quad (33)$$

In Equation (33), ρ_{il} is defined in Equation (22), and Equation (31) can be written as Equation (34) by utilizing the direct neural network robust adaptive fault-tolerance law Equation (19) and control gain Equation (27).

$$\begin{aligned} \frac{dV_1(t)}{dt} &\leq 2 \sum_{i=1}^N \hat{\Omega}_i \|s_{lide}^T PB_2\| s_{lide}^T PB_2 \text{sgn}(s_{lide}^T PB_2)^T \\ &+ 2 \sum_{i=1}^N s_{lide} PB_1 \omega_i + 2s_{lide}^T (I \otimes P) \sum_{i=1}^N \sum_{l=1}^n B_i (\bar{e}_{sil} + \rho_{il} e_{sil} - \rho_{il} \bar{e}_{sil}) \\ &+ 2s_{lide}^T (I \otimes P) \sum_{i=1}^N \sum_{l=1}^n B_i k_{2l} (\hat{e}_{sil} + \rho_{il} \hat{e}_{sil} - \rho_{il} \hat{e}_{sil}) \\ &+ \sum_{i=1}^N \frac{2\Delta\Omega_i}{\gamma_i} \cdot \frac{d\Delta\Omega_i}{dt} + \sum_{i=1}^N \sum_{l=1}^n \frac{2(1-\rho_{il})\Delta\bar{e}_{sil}}{\xi_{ilmax}} \cdot \frac{d\Delta\bar{e}_{sil}}{dt} \\ &+ \sum_{i=1}^N \sum_{l=1}^n \frac{2\rho_{il}\Delta e_{sil}}{\xi_{ilmin}} \cdot \frac{d\Delta e_{sil}}{dt} \\ &\leq 2 \sum_{i=1}^N \hat{\Omega}_i \|s_{lide}^T PB_2\| s_{lide}^T PB_2 \text{sgn}(s_{lide}^T PB_2)^T \\ &+ 2 \sum_{i=1}^N \|s_{lide}^T PB_1\| \|\omega_i\| + \sum_{i=1}^N \frac{2\Delta\Omega_i}{\gamma_i} \cdot \frac{d\Delta\Omega_i}{dt} \end{aligned} \quad (34)$$

From Equation (20), the inequality $s_{lide}^T P B_2 \text{sgn}(s_{lide}^T P B_2)^T \leq -\|s_{lide}^T P B_2\|$ always holds, then Equation (35) holds according to Equations (18) and (19).

$$\begin{aligned} \frac{dV_1(t)}{dt} &\leq -\sum_{i=1}^N \left(2\hat{\Omega}_i \|s_{lide}^T P B_2\|^2 - \|s_{lide}^T P B_1\|^2 - \gamma_i \|s_{lide}\|^2 \right) \\ &+ \sum_{i=1}^N \left(\|\omega_i\|^2 - \gamma_i \|s_{lide}\|^2 \right) + \sum_{i=1}^N \frac{2\Delta\Omega_i}{\gamma_i} \cdot \frac{d\Delta\Omega_i}{dt} \\ &= \sum_{i=1}^N \left(\|\omega_i\|^2 - \gamma_i \|s_{lide}\|^2 \right) \end{aligned} \quad (35)$$

Obviously, assuming $\|s_{lide}\| \geq \frac{\|\omega_i\|}{\sqrt{\gamma_i}}$, we have $\frac{dV_1(t)}{dt} < 0$, implying that the air-ground wireless self-organizing network signals are consistent and ultimately bounded, as shown in Equation (36).

$$\lim_{t \rightarrow \infty} \|s_{lide}\| \in \left\{ s_{lide} \in R^n \mid \|s_{lide}\| \geq \frac{\|\omega_i\|}{\sqrt{\gamma_i}} \right\} \quad (36)$$

For inequality (35), integrating with the interval $t \in [0, \infty)$ is as shown in Equation (37).

$$V_1(t) - V_1(t_0) \leq \sum_{i=1}^N \left(-\int_0^\infty \gamma_i \|s_{lide}(\tau)\|^2 d\tau + \int_0^\infty \|\omega_i(\tau)\|^2 d\tau \right) \quad (37)$$

Equation (38) can be obtained from Equation (37).

$$\sum_{i=1}^N \int_0^\infty \gamma_i \|s_{lide}(\tau)\|^2 d\tau \leq V_1(t_0) + \sum_{i=1}^N \int_0^\infty \|\omega_i(\tau)\|^2 d\tau \quad (38)$$

Equation (38) defines the relevant parameters as shown in Equation (39).

$$\begin{aligned} V_1(t_0) &= s_{lide}^T(t_0) (I \otimes P) s_{lide}(t_0) + \sum_{i=1}^N \frac{\Delta\Omega_i^2(t_0)}{\gamma_i} \\ &+ \sum_{i=1}^N \sum_{l=1}^n \frac{(1-\rho_{il})\Delta\bar{e}_{sil}^2(t_0)}{\xi_{il\max}} + \sum_{i=1}^N \sum_{l=1}^n \frac{\rho_{il}\Delta\underline{e}_{sil}^2(t_0)}{\xi_{il\min}} \end{aligned} \quad (39)$$

Assuming that the initial value of 0 is selected, the L_2 gain can be expressed as Equation (40).

$$\begin{aligned} \gamma_i \int_0^\infty \|s_{lide}(\tau)\|^2 d\tau &\leq \frac{\Delta\Omega_i^2(t_0)}{\gamma_i} + \int_0^\infty \|\omega_i(\tau)\|^2 d\tau \\ &+ \sum_{l=1}^n \frac{(1-\rho_{il})\Delta\bar{e}_{sil}^2(t_0)}{\xi_{il\max}} + \sum_{l=1}^n \frac{\rho_{il}\Delta\underline{e}_{sil}^2(t_0)}{\xi_{il\min}} \end{aligned} \quad (40)$$

Since $\omega_i \in L_2^m[0, \infty)$, we denote $\int_0^\infty \|\omega_i(\tau)\|^2 d\tau < \infty$, and then we have $\int_0^\infty \|s_{lide}(\tau)\|^2 d\tau < \infty$ according to Equation (41). Invoking Barbalat's Lemma [27,28], we have $\lim_{t \rightarrow \infty} s_{lide}(t) = 0$, i.e., the error Δx converges asymptotically to zero. And, it can be guaranteed that Equation (41) holds.

$$\begin{cases} \lim_{t \rightarrow \infty} \frac{d\Omega_i(t)}{dt} = 0 \\ \lim_{t \rightarrow \infty} \frac{d\bar{e}_{si}(t)}{dt} = 0 \\ \lim_{t \rightarrow \infty} \frac{d\underline{e}_{si}(t)}{dt} = 0 \end{cases} \quad (41)$$

According to Equation (40) and references [29–31], the disturbance attenuation L_2 gain level in integrated wireless ad hoc network systems can be ensured to be a sufficiently

small value controlled by γ_i . For $\frac{dV_2(t)}{dt}$, based on Equations (17), (21), and (32), we can derive Equation (42).

$$\begin{aligned} 2\Delta W_F^T \hat{W}_F &= \Delta W_F^T (\Delta W_F + W_F^*) + (\hat{W}_F - W_F^*)^T \hat{W}_F \\ &= \Delta W_F^T \hat{W}_F + (\hat{W}_F - W_F^*)^T W_F^* + \hat{W}_F^T \hat{W}_F - W_F^{*T} \hat{W}_F \\ &= \|\hat{W}_F\|^2 + \|\Delta W_F\|^2 - \|W_F^*\|^2 \geq \|\Delta W_F\|^2 - \|W_F^*\|^2 \end{aligned} \tag{42}$$

Based on the derivation, we can also obtain Equation (43).

$$\begin{cases} \frac{d(t)}{\beta(x)} E_{err} \leq \frac{E_{err}^2}{\varepsilon \beta^2(x)} + \frac{\varepsilon d^2(t)}{4} \\ |\mu_{NI} E_{err}| \leq \frac{E_{err}^2}{2\varepsilon \beta(x)} + \frac{\varepsilon}{2} \mu_{NI}^2 \beta(x) \leq \frac{E_{err}^2}{2\varepsilon \beta(x)} + \frac{\varepsilon}{2} \mu_{NI}^2 \bar{\beta} \end{cases} \tag{43}$$

Since $|\mu_{NI}| \leq \mu_{N0}$, $|d(t)| \leq d_0$, Equation (44) holds.

$$\begin{aligned} \frac{dV_2(t)}{dt} &\leq \\ &-\frac{E_{err}^2}{2\varepsilon \beta^2(x)} - \frac{\sigma}{2} \|\Delta W_F\|^2 + \frac{\varepsilon}{2} \mu_{N0}^2 \bar{\beta} + \frac{\varepsilon}{4} d_0^2 + \frac{\sigma}{2} \|W_F^*\|^2 \end{aligned} \tag{44}$$

In this case, since $\Delta W_F^T \Gamma^{-1} \Delta W_F \leq \bar{\gamma} \|\Delta W_F\|^2$ and $\bar{\gamma}$ represents the maximum eigenvalue of Γ^{-1} , Equation (45) holds.

$$\frac{dV_2(t)}{dt} \leq -\frac{1}{\alpha_0} V_2(t) + \frac{\varepsilon}{2} \mu_{N0}^2 \bar{\beta} + \frac{\varepsilon}{4} d_0^2 + \frac{\sigma}{2} \|W_F^*\|^2 \tag{45}$$

Equation (45) states that $\alpha_0 = \max\{\varepsilon, \frac{\sigma}{2}\}$. If we solve the inequality in Equation (45), we have Equation (46) holding.

$$\begin{cases} \frac{dV_2(t)}{dt} \leq e^{-\frac{t}{\alpha_0}} V_2(0) + \alpha_0 \left(\frac{\varepsilon}{2} \mu_{N0}^2 \bar{\beta} + \frac{\varepsilon}{4} d_0^2 + \frac{\sigma}{2} \|W_F^*\|^2 \right) \\ t \geq 0 \end{cases} \tag{46}$$

In Equation (46), since $V_2(0)$ is bounded, the inequality (46) implies that both E_{err} and $\hat{W}_F(t)$ are bounded. By Equation (29), it follows that $V_2(t) \geq \frac{E_{err}^2}{2\beta(x)}$, and, consequently, Equation (47) holds.

$$E_{err} \leq \sqrt{2\beta(x)V_2(t)} \leq \sqrt{2\bar{\beta}V_2(t)} \tag{47}$$

By combining Equation (46) along with the inequality $\sqrt{ab} \leq \sqrt{a} + \sqrt{b} (a > 0, b > 0)$, we can conclude that Equation (48) holds.

$$\begin{cases} |E_{err}| \leq \\ e^{-\frac{t}{2\alpha_0}} \sqrt{2\bar{\beta}V_2(0)} + \sqrt{\alpha_0 \bar{\beta}} \cdot \sqrt{\varepsilon \mu_{N0}^2 \bar{\beta} + \frac{\varepsilon}{2} d_0^2 + \sigma \|W_F^*\|^2} \\ t \geq 0 \end{cases} \tag{48}$$

The proof is complete. \square

Moreover, similar to the proof of Theorem 1, according to Equation (33), Equation (49) holds if and only if $s_{lide} = 0$.

$$s_{lide}^T (I \otimes P) \sum_{i=1}^N \sum_{i=1}^n B_i f_l e_{sil} = s_{lide}^T (I \otimes P) \sum_{i=1}^N \sum_{i=1}^n B_i f_l (\bar{e}_{sil} + \rho_{il} e_{sil} - \rho_{il} \bar{e}_{sil}) \tag{49}$$

And $\frac{dV_1(t)}{dt} = 0$ if and only if $s_{lidei} = 0, i = 1, 2, \dots, N$. A set as shown in Equation (50) can be found.

$$C_E = \left\{ (s, \hat{e}, \hat{e}) : \frac{dV_1(t)}{dt} = 0 \right\} = \left\{ (s, \hat{e}, \hat{e}) : s_{lidei} = 0 \right\} \quad (50)$$

where, in Equation (50), the relevant parameters are defined as shown in Equation (51).

$$\begin{cases} s = (s_1, \dots, s_N)^T \\ \hat{e} = (\hat{e}_1, \dots, \hat{e}_N)^T \\ \hat{e} = (\hat{e}_1, \dots, \hat{e}_N)^T \end{cases} \quad (51)$$

Starting from any initial value $s_1(0), \hat{e}(0), \hat{e}(0)$, the ideal target optimal trajectory converges asymptotically and stably to $s_1 = 0, \hat{e}_i = \underline{e}_i, \hat{e}_i = \bar{e}_i$, where $\underline{e}_i, \bar{e}_i$ is a constant. Based on the LaSalle invariant set principle, the optimal tracking trajectory of the network system converges to the maximum positive invariant subset $M_E = \left\{ (s, \hat{e}, \hat{e}) : s = 0, \frac{d\hat{e}}{dt} = 0, \frac{d\hat{e}}{dt} = 0 \right\}$. According to Equations (11) and (31), it can be found that the system error converges asymptotically to 0. It is assumed that there exists Q_1 and P such that inequality (16) holds.

4. Simulation and Experiment Test Analysis

4.1. Simulation Analysis

In this paper, MATLAB software is used for simulation verification and analysis to simulate and test the performance of the controller designed in this paper, and the following initial conditions are given in reference [32–34]. The overall simulation time is 50 s. Considering an extensive system composed of two identical air–ground integrated dynamic subsystems, the relevant parameters are defined in Equation (52). For the sake of generality, both “System 1” and “System 2” in the simulation analysis of this paper contain four subsystems with the same dynamics.

$$\begin{cases} A = \begin{bmatrix} -1.24 & 0.261 \\ 1 & 0.124 \end{bmatrix}, B_1 = \begin{bmatrix} 1.2461 & 1 \\ -2.14 & -1.24 \end{bmatrix} \\ A_1 = \begin{bmatrix} 0.61 & 0 \\ 0 & 0.61 \end{bmatrix}, B_2 = \begin{bmatrix} 2.14 & -1.2461 \\ 1 & -1.24 \end{bmatrix} \end{cases} \quad (52)$$

The air–ground integrated wireless mobile self-organizing network topology matrix L is defined in Equation (53).

$$L = \begin{bmatrix} -1.24 & 0.223 & 0.567 & 0.312 \\ 0.161 & -1.24 & 0.611 & 0.337 \\ 0.215 & 0.497 & -1.24 & 0.342 \\ 0.117 & 0.312 & 0.611 & -1.24 \end{bmatrix} \quad (53)$$

The simulation parameters and initial values in Equation (54) are given.

$$\begin{cases} \gamma_i = 124, \quad \xi_{il\max} = 100, c = 0.99 \\ \Delta \bar{e}_{sil} = 12, \quad \Delta \underline{e}_{sil}(0) = -12 \\ x_1(0) = [2, -1.0]^T, \quad x_2(0) = [1, -0.5]^T \\ x_3(0) = [0.5, -1.5]^T, \quad x_4(0) = [0.5, -3]^T \end{cases} \quad (54)$$

The MATLAB 2020b software was used to solve the LMI to obtain Equation (55).

$$\begin{cases} P = \begin{bmatrix} 0.1261 & -0.0214 \\ -0.0214 & 0.0278 \end{bmatrix} \\ K_1 = \begin{bmatrix} 1.8127 & -2.6914 \\ 1.8127 & -3.6641 \end{bmatrix} \end{cases} \quad (55)$$

This paper considers the following two modes: one for normal operation and one for faulty operation. They are described as follows.

Simulation Test 1

(1) Cooperative flight control of UAV subsystems in normal operation mode: all the subsystems are in normal operation mode. To show the performance of the controller intuitively, this paper makes the ideal output values of the quadcopter UAV set as follows: the three significant angles of the subsystem 1 are 80, 60, and 40, respectively; the three significant angles of the subsystem 2 are -90 , -70 , and -50 , respectively. Then, the simulation can be obtained as shown in Figure 1.

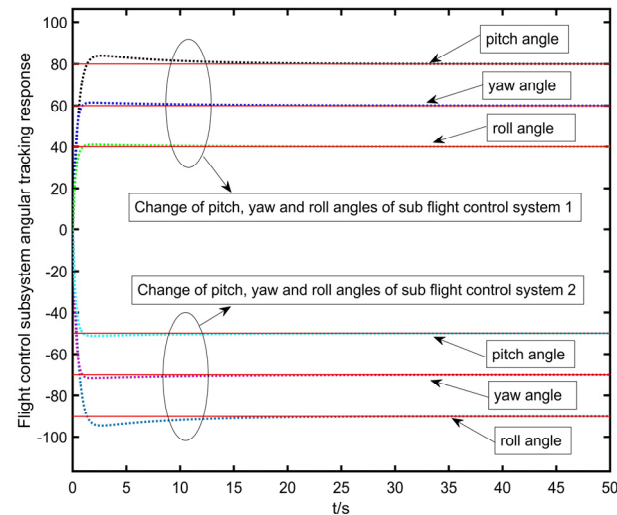


Figure 1. UAV subsystem flight control in normal operating mode.

From Figure 1, it is very intuitive to see that when the subsystems are all in regular operation, the overall flight control performance can reach the ideal output state very accurately under the feedback control of the controller designed in this paper.

(2) Subsystem wireless self-organizing network association link in normal working mode: all the subsystem wireless self-organizing network association links are in normal working mode. To show the performance of the controller intuitively, this paper makes the ideal output value of the wireless self-organizing network association link set as follows: the response of the association link of subsystem 1 is $2.5 \sin(t)$; the reaction of the association link of subsystem 2 is $1.5 \sin(t)$; the answer of the association link between subsystem 1 and subsystem 2 is $0.5 \sin(t)$. Then, the simulation curve, as shown in Figure 2, can be obtained.

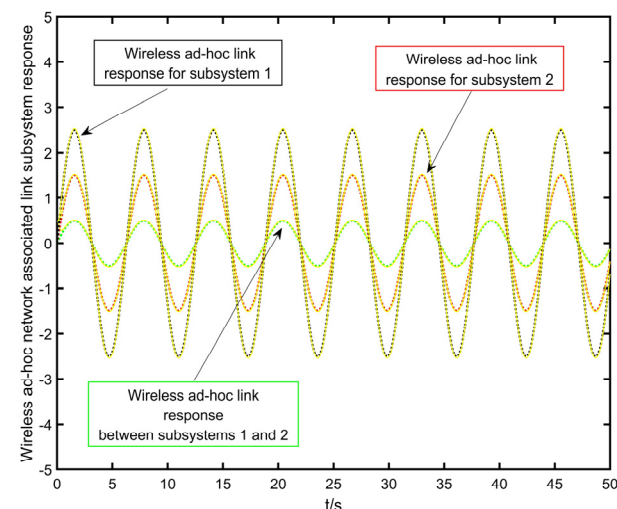


Figure 2. Wireless self-organizing network association links of subsystems in normal operating mode.

From Figure 2, it is intuitive to see that when the subsystems are all in regular operation, the overall wireless self-organizing network association link performance can reach the ideal output state precisely under the feedback control of the controller designed in this paper.

Simulation Test 2

(1) Cooperative flight control of UAV subsystems in faulty operation mode: All subsystems are in normal operation mode. Subsystem 1 suffers from sudden interruption failure of the internal actuator of the UAV and random time delay failure of wireless self-organized network communication at the 10th and 30th seconds simultaneously, and the failure continues until the end of the simulation; subsystem 2 suffers from the partial failure of the internal actuator of the UAV and slight probability of packet loss failure of wireless self-organized network communication at the 20th and 40th seconds simultaneously. Subsystem 2 suffers from a partial failure of the internal actuator of the UAV and a small probability of packet loss in the wireless self-organizing network communication at the 20th and 40th seconds, and the failure continues until the end of the simulation. To visualize the controller's performance, this paper makes the ideal output value setting of the quadcopter UAV consistent with the ordinary operation mode, and the perfect output value setting of the wireless self-organized network association link compatible with the ordinary operation mode. Then, the simulation curves can be obtained, as shown in Figures 3–7.

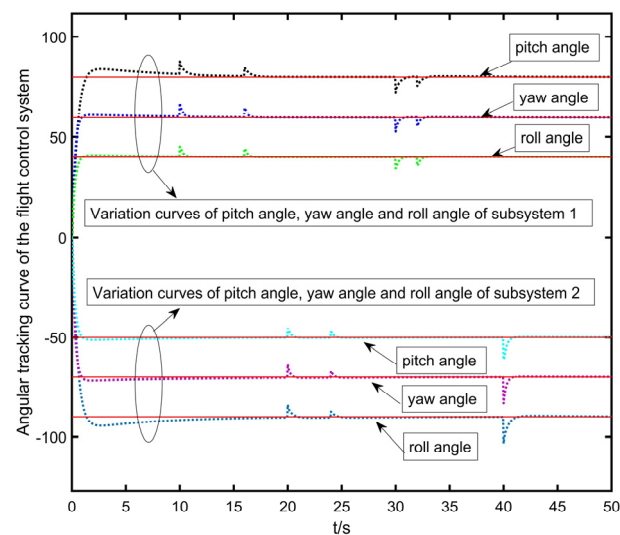


Figure 3. UAV subsystem flight control in failure mode.

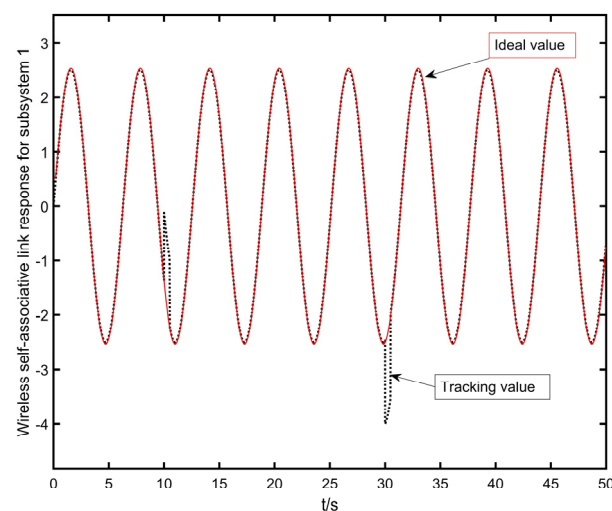


Figure 4. Wireless correlation failure mode for subsystem 1.

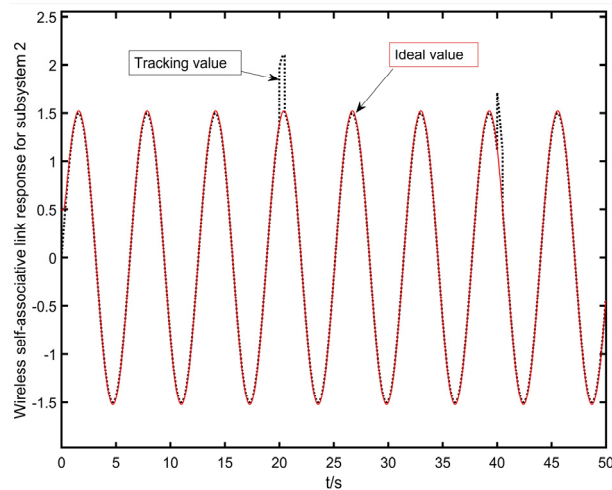


Figure 5. Wireless correlation failure mode for subsystem 2.

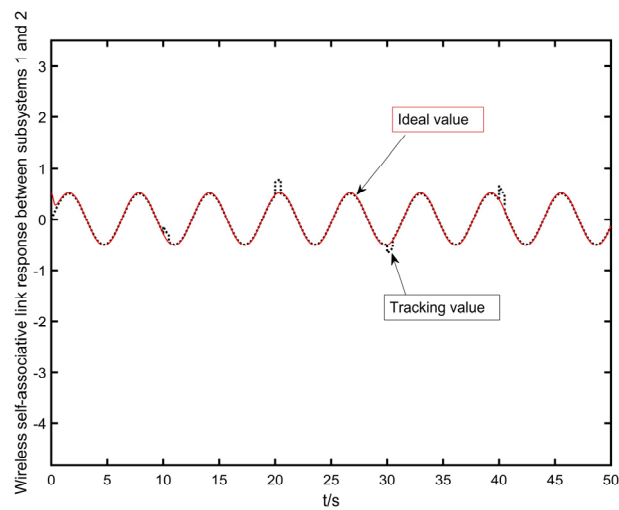


Figure 6. Wireless correlation failure modes for subsystems 1 and 2.

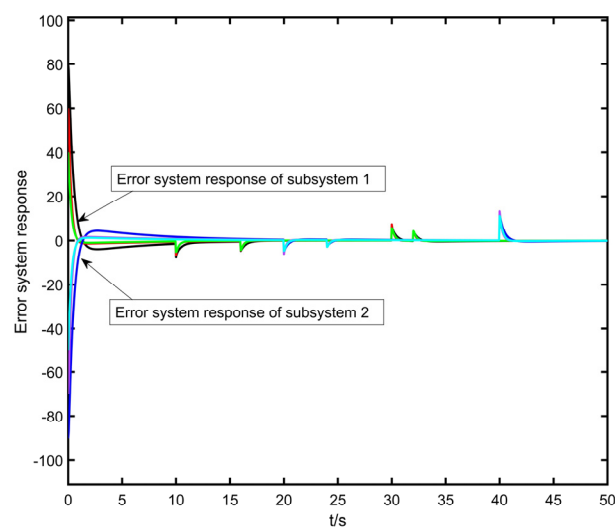


Figure 7. Overall tracking error system in subsystem 1 and subsystem 2 failure modes.

Figure 3 shows that a total of 4 peaks and three troughs (defining upward fluctuations of the curve as peaks and downward fluctuations as troughs) occur when subsystem 1 and subsystem 2 encounter faulty disturbances during the simulation. Among them, for

subsystem 1, between 10 s and 20 s, two wave peaks appeared in the three significant angles of the quadcopter UAV, with mountains of 85.74, 63.65, and 42.14, and 83.56, 61.44, and 41.76, and fluctuation errors of +5.74, +3.65, and +2.14, and +3.56, +1.44, and +1.76, respectively, and between 30 s and 35 s, there are two troughs in the three significant angles of the quadcopter UAV, with tracks of 72.31, 51.97, 33.77, 76.75, 56.72, 36.58, and fluctuation errors of -7.69 , -8.03 , -6.23 , and -3.25 , -3.28 , -3.42 , respectively. For subsystem 2, between 20 s and 25 s, the three significant angles of the quadcopter UAV appeared as two wave peaks, with peaks: -47.19 , -63.78 , -86.97 ; -48.27 , -68.44 , -89.23 , and fluctuation errors: +2.81, +6.22, +3.03; +1.73, +1.56, 0.77, respectively, and at the 40th s, the three major quadcopter UAV angles appear in one trough; the troughs are -63.21 , -88.64 , -102.37 , and the fluctuation errors are -13.21 , -18.64 , -12.37 , respectively. In summary, the fluctuation errors are within the allowable range, i.e., the three significant angles of the quadcopter UAVs of subsystem 1 and subsystem 2, the pitch, the roll, and the yaw angles can be gradually stabilized and accurately reach the system's expected values with the designed controllers, and the system's desired values can be precisely achieved with the designed controllers stabilization and accurately reach the desired values of the system.

From Figure 4, it can be intuitively seen that, for subsystem 1, the wireless self-organizing network association link has one peak at the 10th s, with a fluctuation error of +1.51, and one trough at the 30th s, with a fluctuation error of -1.47 . The fluctuation errors are all in the permissible range, i.e., the wireless self-organizing network association link of subsystem 1 can be gradually stabilized along with the designed controller and accurately meet the desired value of the system. They stabilize and accurately reach the expected value of the system.

From Figure 5, it can be seen very intuitively that for subsystem 2, there is one wave peak with a fluctuation error of +0.58 for the wireless self-organizing network association link at 20 s and one wave peak with a fluctuation error of +0.49 at 40 s. The fluctuation errors are all within the permissible range, i.e., the wireless self-organizing network association link of subsystem 2 can gradually stabilize with the designed controller to reach the system's accurately desired value.

From Figure 6, it can be intuitively seen that for the wireless self-organizing network association link between subsystem 1 and subsystem 2, there are three peaks and one trough between the 10th and 40th s, with fluctuation errors of +0.24, +0.37, -0.26 , and +0.32, respectively. The fluctuation errors are within the permissible range, i.e., the wireless self-organizing network association link between subsystem 1 and subsystem 2 can gradually stabilize with the designed controller to reach the desired value of the system accurately.

From Figure 7, it can be seen very intuitively that the overall tracking error system under the failure modes of subsystem 1 and subsystem 2 can be adjusted with the feedback control of the controller designed in this paper. After a short period of feedback adjustment, the error asymptotically converges to zero and finally reaches a stable state.

4.2. Experiment Test Analysis

To verify the practical application performance of the controller designed in this paper, the experimental equipment shown in Figure 8 is used in this paper, and the field experiment contains one signal source node, two airborne relay self-organizing network nodes, one vehicle-mounted relay self-organizing network node, and one letter-host self-organizing network node. Among them, the wireless self-organizing network node self-organizing network protocol is 802.15.4, the operating frequency is 2.4 GHz, and the UAV models are M100 and W100. The maximum moving speed of the air self-organizing network node 1 is 91 km/h, the maximum moving speed of the air self-organizing network node 2 is 65 km/h, the maximum moving speed of the vehicle self-organizing network node 1 is 70 km/h, and the transmission distance between nodes range $d \in [8, 10]$ km. Compared to the analysis of simulation results, the performance of the controller cannot be fully reflected from the generality at present due to the limitation of the experimental equipment, but this paper has provided three mobile self-organizing nodes as far as possible, including one

ground mobile organizing node and two airmobile organizing nodes. This research team will continue to conduct in-depth research and discuss the subsequent purchase plan and will improve the general experimental results as much as possible in future research.

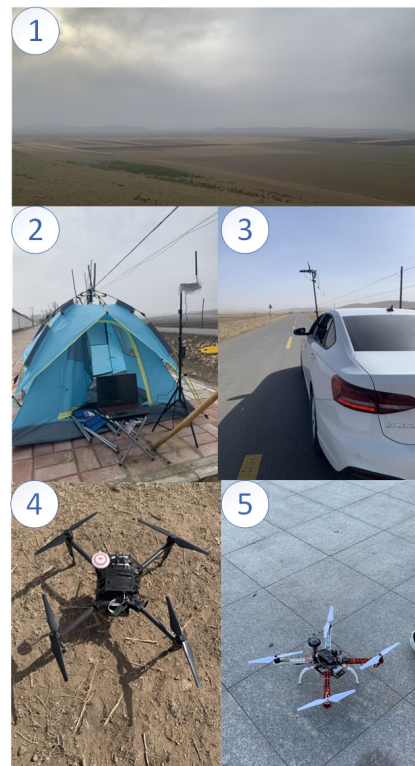


Figure 8. The overall experimental framework structure.

As shown in Figure 8, ① denotes the experimental test environment. ② denotes the signal source node. ③ denotes the on-board signaling node. ④ denotes the air self-organizing network node 1: M100. ⑤ denotes the air self-organizing network node 2: W100, where the signal source network node is numbered as “65CB”, the vehicle network node is numbered as “65FD”, the air network node one is numbered as “5F0C”, and the air network node two is numbered as “A 5F0C”, and air network node two is numbered “A230”. In the first test, without adding the controller designed in this paper, there is a wireless self-organizing network topology shown in Figure 9.

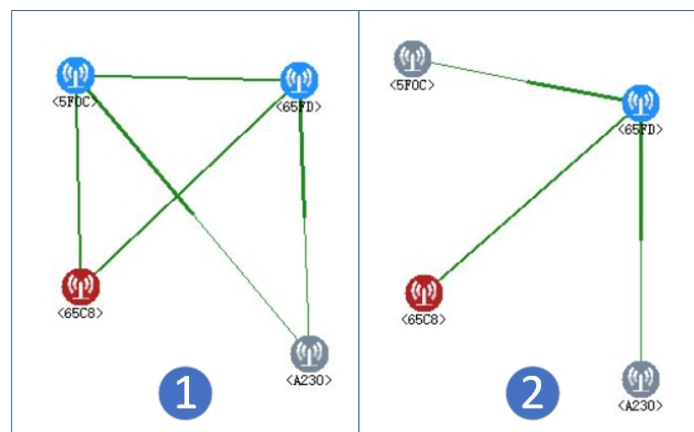


Figure 9. Wireless self-organizing network topology without adding the controller designed in this paper.

It can be intuitively seen from Figure 9 that when the controller designed in this paper is not added, when the highest moving speed of the vehicle-based networking node is 70 km/h, the highest moving rate of the airborne networking node 1 is 91 km/h, the highest moving speed of the airborne networking node 2 is 65 km/h. The communication distance between the networking nodes is up to 10,000 m, and the unknown topology of the networking topology occurs in the process of the network test. When interference occurs, the air-ground integrated wireless self-organizing network topology appears to have two kinds of abnormal and unstable topologies, which seriously affect the performance index of wireless self-organizing network nodes. The ① in Figure 9 represents the irregular topology 1, and the ② in Figure 9 illustrates the irregular, unstable topology 2. Then, the wireless self-organizing network topology is tested when the controller designed in this paper is added, as shown in Figure 10.

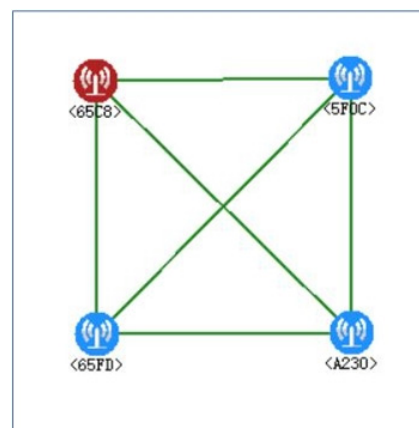


Figure 10. Wireless self-organizing network topology when adding the controller designed in this paper.

The experimental environment and experimental parameter settings in Figure 10 are consistent with those in Figure 9. From Figure 10, it can be intuitively seen that by adding the controller designed in this paper, the air-ground integrated wireless self-organizing network topology is stable and reliable, and the wireless self-organizing network nodes all usually work with good performance. Comparing with Figure 9, it can be seen that the stability of the wireless self-organizing network topology is significantly improved, in which the strength of the performance is maximally enhanced by 50%.

5. Conclusions and Outlook

5.1. Conclusions

This paper takes the air-ground integrated wireless mobile self-organizing network cluster system as the research object, based on the neural network intelligent control and robust adaptive fault-tolerant control theory, designs the intelligent, cooperative fault-tolerant controller applicable to the mobile cluster system under the long-distance transmission, and from the simulation results: the cluster subsystem, in the face of the wireless mobile self-organizing network communication faults and the unknown faults of its actuator, the dynamic fluctuation of rotary-wing UAV in the subsystem is within the permissible error range. The emotional change of the wireless self-organized network association link among the three angles/subsystems is within the allowable error range, and the cluster system conforms to the asymptotic stabilization principle and shows good robustness, fault tolerance, and self-learning adaptive regulation, which provides a specific research basis for the subsequent research. From the experimental results: when the farthest transmission distance between nodes of air-ground self-organizing network is 10 km, and the nodes move at the speed interval of [0, 91] km/h, the overall loop success rate of air-ground integrated clustered mobile grouping system is relatively stable, with minor fluctuations,

the wireless self-organizing network signal transmission is relatively stable, and the wireless self-organizing network topology is stable, which is of particular application value. The controller proposed in this paper effectively improves the long-distance transmission performance of air-ground integrated wireless high-mobility self-organizing network, and this paper provides a certain research basis for the future multi-intelligent flying networking economic system, and the fields involved include border patrol, forest fire prevention, unmanned courier in the air-ground, post-disaster reconstruction, and early warning of accidents.

5.2. Outlook

In this paper, we design an intelligent, cooperative fault-tolerant controller for the long-distance transmission of a high-mobility trunking system, which achieves good results in simulation and experiments for the long-distance trunking transmission system of air-ground integrated wireless high-mobility self-organizing network. The controller designed in this paper still has certain deficiencies from a long-term perspective, such as how to realize cooperative computation, control, and decision-making among bits of intelligence on the edge networking nodes; how to ensure the robustness and safety of air-ground integrated wireless high-mobility self-organizing network system in the long-distance transmission process, etc., which still needs to be in-depth and closely combined with the discipline of artificial intelligence, and take into account the close connection of reinforcement learning, deep learning, edge computing, and other technologies. Computing and other technologies are closely linked. This paper also provides a specific research basis for the stability control of multi-intelligent body clusters under the long-distance transmission of an air-ground integrated wireless high-mobility self-organizing network system.

Author Contributions: Conceptualization, Z.W. and J.Y.; methodology, Z.W.; software, Y.B.; validation, Q.H., W.X. and M.S.; formal analysis, M.S.; investigation, X.H.; resources, M.S.; data curation, Z.W.; writing—original draft preparation, Z.W.; writing—review and editing, Z.W.; visualization, Y.B.; supervision, Y.B.; project administration, Q.H.; funding acquisition, J.Y. All authors have read and agreed to the published version of the manuscript.

Funding: This project was partly supported by the Henan Provincial Science and Technology Tackling Projects 242102210212 (Financier: Dr Zhifang Wang), 242102311217 (Financier: Dr Wenke Xu) and supported by the Open Subjects of Key Cultivation Laboratory of Intelligent Transportation Policing in Henan Police Academy ZHJT202403 (Financier: Dr Zhifang Wang) and supported by the National Natural Science Foundations of China under grants 62173126 (Financier: Prof Quanzhen Huang), 61821001 (Financier: Prof Jianguo Yu), and 62127802 (Financier: Prof Jianguo Yu) and supported by the Central Plains Science and Technology Innovation Leader Support Program under grant 234200510027 (Financier: Prof Quanzhen Huang).

Data Availability Statement: We solemnly declare the following when collecting, processing, and using data: Purpose of data collection: We clearly inform our users of the purpose of our data collection and how it will be used, and that the data will be collected only to the extent necessary to provide the service or improve the user experience. Lawful basis: We comply with the applicable laws and regulations and only collect and use data as permitted by law. Data security: We take reasonable measures to ensure the security of user data and to prevent unauthorized access, use or disclosure. Informed consent of users: We will obtain the informed consent of users after clearly informing them of the purpose, manner and scope of data use. Data sharing: We will not share the user's personal data with third parties unless we have the user's explicit consent or are required by law or regulation. Anonymization and data retention: We anonymize personal data and strictly control the retention period of the data to ensure that it does not last longer than necessary. Transparency and the right to information: We will provide a transparent privacy policy that clearly describes our data processing practices, as well as the rights and choices of our users regarding the use of their data. Review and update: We will regularly review and update our data use policy to ensure consistency with the latest laws and regulations and ethical principles.

Conflicts of Interest: The authors declare no conflicts of interest.

References

1. Zou, Y.; Xia, K. Robust Fault-Tolerant Control for Underactuated Takeoff and Landing UAVs. *IEEE Trans. Aerosp. Electron. Syst.* **2020**, *56*, 3545–3555. [[CrossRef](#)]
2. Liu, D.; Liu, H.; Lewis, F.L.; Wan, Y. Robust Fault-Tolerant Formation Control for Tail-Sitters in Aggressive Flight Mode Transitions. *IEEE Trans. Ind. Inform.* **2020**, *16*, 299–308. [[CrossRef](#)]
3. Chen, F.; Jiang, R.; Zhang, K.; Jiang, B.; Tao, G. Robust Backstepping Sliding-Mode Control and Observer-Based Fault Estimation for a Quadrotor UAV. *IEEE Trans. Ind. Electron.* **2016**, *63*, 5044–5056. [[CrossRef](#)]
4. Wang, Z.; Huang, Q.; Yu, J. Neural network-based direct robust adaptive non-fragile fault-tolerant control of amorphous flattened air-ground wireless self-assembly system. *Robot. Intell. Autom.* **2023**, *43*, 537–550. [[CrossRef](#)]
5. Wang, Z.; Yu, J.; Lin, S. Bidirectional Robust and Fault-tolerant H_∞ Non-sensitive Compensation Filter Controller based on Amorphous Flattened Air-to-ground Wireless Self-assembly System. *ISA Trans.* **2023**, *132*, 508–523. [[CrossRef](#)] [[PubMed](#)]
6. Zhou, X.; Hou, H.; Liang, W.; Wang, K.I.-K.; Jin, Q. Intelligent Containment Control with Double Constraints for Cloud-Based Collaborative Manufacturing. *IEEE Trans. Ind. Inform.* **2023**, *19*, 7541–7551. [[CrossRef](#)]
7. He, W.; Sun, Y.; Yan, Z.; Yang, C.; Li, Z.; Kaynak, O. Disturbance Observer-Based Neural Network Control of Cooperative Multiple Manipulators with Input Saturation. *IEEE Trans. Neural Netw. Learn. Syst.* **2020**, *31*, 1735–1746. [[CrossRef](#)] [[PubMed](#)]
8. Liu, L.; Song, S.; Wang, Z. A Novel Interleaving Scheme for Concatenated Codes on Burst-Error Channel. In Proceedings of the 2022 27th Asia Pacific Conference on Communications (APCC), Jeju Island, Republic of Korea, 19–21 October 2022; pp. 309–314. [[CrossRef](#)]
9. Li, J.; Reviriego, P.; Xiao, L.; Wu, H. Protecting Memories against Soft Errors: The Case for Customizable Error Correction Codes. *IEEE Trans. Emerg. Top. Comput.* **2021**, *9*, 651–663. [[CrossRef](#)]
10. Liu, H.; Reviriego, P.; Argyrides, C.; Xiao, L. Correction Masking: A Technique to Implement Efficient SET Tolerant Error Correction Decoders. *IEEE Trans. Device Mater. Reliab.* **2022**, *22*, 36–41. [[CrossRef](#)]
11. Zhang, J.; Jiang, Y.; Liu, X.; Lee, M.; Gao, H.; Yu, G. Design of Retransmission Mechanism for Decentralized Inference with Graph Neural Networks. In Proceedings of the 2022 27th Asia Pacific Conference on Communications (APCC), Jeju Island, Republic of Korea, 19–21 October 2022; pp. 515–519. [[CrossRef](#)]
12. Hourani, K.; Pandurangan, G.; Robinson, P. Awake-Efficient Distributed Algorithms for Maximal Independent Set. In Proceedings of the 2022 IEEE 42nd International Conference on Distributed Computing Systems (ICDCS), Bologna, Italy, 10–13 July 2022; pp. 1338–1339. [[CrossRef](#)]
13. Vaz, D.; Matos, D.R.; Pardal, M.L.; Correia, M. Automatic Generation of Distributed Algorithms with Generative AI. In Proceedings of the 2023 53rd Annual IEEE/IFIP International Conference on Dependable Systems and Networks—Supplemental Volume (DSN-S), Porto, Portugal, 27–30 June 2023; pp. 127–131. [[CrossRef](#)]
14. Haiyang, M.; Changchun, Z.; Guangshan, C.; Chenglong, J.; Yiyang, P.; Yangxiu, H. Research on Object Positioning Algorithm Based on Hybrid Monocular-Binocular. In Proceedings of the 2023 42nd Chinese Control Conference (CCC), Tianjin, China, 24–26 July 2023; pp. 7471–7477. [[CrossRef](#)]
15. Zhang, D.; Tang, Y.; Zhang, W.; Wu, X. Hierarchical Design for Position-Based Formation Control of Rotorcraft-Like Aerial Vehicles. *IEEE Trans. Control Netw. Syst.* **2020**, *7*, 1789–1800. [[CrossRef](#)]
16. Hui, Y.; Jianxiong, W.; Jianbo, S.; Shiwei, F.; Fei, Y.; Wenjun, H. Research on AUV Cooperative Positioning Technology Based on Improved-EKF With Error Estimation. In Proceedings of the 2021 33rd Chinese Control and Decision Conference (CCDC), Kunming, China, 22–24 May 2021; pp. 391–396. [[CrossRef](#)]
17. Fu, J.; Zhang, L.; Wang, L.; Li, F. BCT: An Efficient and Fault Tolerance Blockchain Consensus Transform Mechanism for IoT. *IEEE Internet Things J.* **2023**, *10*, 12055–12065. [[CrossRef](#)]
18. James, B.; Quinn, H.; Wirthlin, M.; Goeders, J. Applying Compiler-Automated Software Fault Tolerance to Multiple Processor Platforms. *IEEE Trans. Nucl. Sci.* **2020**, *67*, 321–327. [[CrossRef](#)]
19. Krishna, K.M.; Sarawadekar, K.P. Design of Concurrent Error Detection Techniques for FFT implemented on FPGA platform. In Proceedings of the 2021 IEEE 18th India Council International Conference (INDICON), Guwahati, India, 19–21 December 2021; pp. 1–7. [[CrossRef](#)]
20. Huang, C.-H.; Chen, W.-J. A Spatial–Temporal Error Spreading Technique Based on Voltage Dithering Demonstrates a Power Savings of 35% in a Real-Time Video Processing Datapath Without Timing-Error Detection and Correction. *IEEE Solid-State Circuits Lett.* **2020**, *3*, 378–381. [[CrossRef](#)]
21. Liu, X.; Lyu, J. Design of Transponder Message Transmission Mechanism Based on Error Correction Code BCH. In Proceedings of the 2021 7th International Conference on Computer and Communications (ICCC), Chengdu, China, 10–13 December 2021; pp. 2127–2131. [[CrossRef](#)]
22. Cohen, A.; D’oliveira, R.G.L.; Duffy, K.R.; Woo, J.; Medard, M. AES as Error Correction: Cryptosystems for Reliable Communication. *IEEE Commun. Lett.* **2023**, *27*, 1964–1968. [[CrossRef](#)]
23. Nakahara, M.; Hisano, D.; Nishimura, M.; Ushiku, Y.; Maruta, K.; Nakayama, Y. Retransmission Edge Computing System Conducting Adaptive Image Compression Based on Image Recognition Accuracy. In Proceedings of the 2021 IEEE 94th Vehicular Technology Conference (VTC2021-Fall), Norman, OK, USA, 27 September–28 October 2021; pp. 1–5. [[CrossRef](#)]
24. Song, T.; Lee, W.-H. HARE: Hybrid ARQ-Based Adaptive Retransmission Control Scheme for Synchronous Multi-Link in Wireless LANs. *IEEE Trans. Veh. Technol.* **2023**, *72*, 10302–10313. [[CrossRef](#)]

25. Cleveland-Slimming, M.; Leger, P. A Collaborative Learning Strategy in an MIS Development Course Using Case Method in Engineering in Information and Management Control. In Proceedings of the 2020 39th International Conference of the Chilean Computer Science Society (SCCC), Coquimbo, Chile, 16–20 November 2020; pp. 1–5. [\[CrossRef\]](#)
26. Heshmati-Alamdari, S.; Nikou, A.; Dimarogonas, D.V. Robust Trajectory Tracking Control for Underactuated Autonomous Underwater Vehicles in Uncertain Environments. *IEEE Trans. Autom. Sci. Eng.* **2021**, *18*, 1288–1301. [\[CrossRef\]](#)
27. Llin, L.; Jia, Q.; Lv, C.; Liang, J.; Luo, P. Partitional Collaborative Mitigation Strategy of Distribution Network Harmonics Based on Distributed Model Predictive Control. *IEEE Trans. Smart Grid* **2023**, *14*, 1998–2009. [\[CrossRef\]](#)
28. Zhang, R.; Liu, Y. A new Barbalat’s lemma and Lyapunov stability theorem for fractional order systems. In Proceedings of the 2017 29th Chinese Control and Decision Conference (CCDC), Chongqing, China, 28–30 May 2017; pp. 3676–3681. [\[CrossRef\]](#)
29. Zhuang, G.; Xia, J.; Feng, J.-E.; Sun, W.; Zhang, B. Admissibilization for Implicit Jump Systems with Mixed Retarded Delays Based on Reciprocally Convex Integral Inequality and Barbalat’s Lemma. *IEEE Trans. Syst. Man Cybern. Syst.* **2021**, *51*, 6808–6818. [\[CrossRef\]](#)
30. Liu, J.; Song, H.; Zhao, Z.; Guerrero, J.M.; Qu, Y. L2-Gain Disturbance Attenuation-Based Decentralized Secondary Frequency Control in Autonomous Microgrids. In Proceedings of the 2022 34th Chinese Control and Decision Conference (CCDC), Hefei, China, 21–23 May 2022; pp. 3162–3167. [\[CrossRef\]](#)
31. Tao, D.; Xiaoyu, G.; Wanquan, L. Disturbance attenuation and rejection for systems with unknown nonlinearity and missing measurements via DOBC approach. In Proceedings of the 2017 36th Chinese Control Conference (CCC), Dalian, China, 26–28 July 2017; pp. 8032–8037. [\[CrossRef\]](#)
32. Liu, J.; Song, H.; Chen, C.; Guerrero, J.M.; Liu, M.; Qu, Y. A Non-linear Decentralized Secondary Frequency Control of islanded Microgrid via Adaptive L2-Gain Disturbance Attenuation. In Proceedings of the 2022 IEEE 31st International Symposium on Industrial Electronics (ISIE), Anchorage, AK, USA, 1–3 June 2022; pp. 448–453. [\[CrossRef\]](#)
33. Li, J.; Zhou, T.; Cui, H. Brain-Inspired Deep Meta-Reinforcement Learning for Active Coordinated Fault-Tolerant Load Frequency Control of Multi-Area Grids. *IEEE Trans. Autom. Sci. Eng.* **2023**, 1–3. [\[CrossRef\]](#)
34. Troubitsyna, E. Formal Model of Collaborative Fault Tolerant Planning in Multi-Robotic Systems. In Proceedings of the 2022 8th International Conference on Control, Decision and Information Technologies (CoDIT), Istanbul, Turkey, 1–3 June 2022; pp. 1438–1443. [\[CrossRef\]](#)

Disclaimer/Publisher’s Note: The statements, opinions and data contained in all publications are solely those of the individual author(s) and contributor(s) and not of MDPI and/or the editor(s). MDPI and/or the editor(s) disclaim responsibility for any injury to people or property resulting from any ideas, methods, instructions or products referred to in the content.